X-rays enhance Fe^{2+}-mediated oxidative membrane damage in OUMS-36T-1 fibroblasts, supported by the liposome model

SHINYA KATO[1]

Radioisotope Experimental Facility, Mie University, Tsu, Mie 514-8507, Japan

Received October 20, 2025; Accepted February 11, 2026

DOI: 10.3892/mi.2026.305

Abstract. Ferroptosis is a regulated form of cell death driven by iron-dependent membrane lipid peroxidation, with ferrous ions (Fe^{2+}) and reactive oxygen species playing central roles. Although X-rays are known to generate free radicals via water radiolysis, their role in ferroptosis-related oxidative membrane injury remains unclear. The present study investigated the effects of Fe^{2+} on membrane damage in OUMS-36T-1 human fibroblasts under X-ray irradiation. DOPC/DOPS (8:2 mol/mol) liposomes were employed as a simplified membrane model to explore the underlying mechanisms. *In vitro*, Fe^{2+} at 1-40 μM promoted cell proliferation up to 10 μM, whereas higher concentrations of Fe^{2+} reduced cell viability. At 40 μM Fe^{2+}, intracellular reactive oxygen species and lipid peroxidation levels were elevated; however, lactate dehydrogenase leakage was not observed, suggesting sublethal oxidative stress without overt membrane rupture. However, following 4 Gy X-ray irradiation, cell proliferation at 40 μM Fe^{2+} significantly decreased, accompanied by increased oxidative stress, lipid peroxidation and lactate dehydrogenase leakage, indicating enhanced membrane damage rather than definitive ferroptotic cell death. These effects were mitigated by citric acid, an iron chelator, or reduced glutathione, suggesting the involvement of redox-dependent processes at or near the membrane surface. Experiments with DOPC/DOPS (8:2 mol/mol) liposomes revealed that Fe^{2+}-induced lipid peroxidation was significantly enhanced by X-rays. Furthermore, the combination of liposomes and X-rays appeared to accelerate the oxidation of Fe^{2+}. These findings suggest that Fe^{2+} interacts with cell membranes to promote lipid peroxidation and impair proliferation, and that X-rays amplify these effects by exacerbating Fe^{2+}-mediated oxidative membrane damage. Given the critical role of fibroblasts in post-irradiation tissue repair, the present study highlights the synergistic impact of Fe^{2+} and X-rays on ferroptosis-associated oxidative membrane injury, underscoring their biological significance.

Correspondence to: Dr Shinya Kato, [1]*Present address:* Kyoto University Institute for Integrated Radiation and Nuclear Science (KURNS), 2, Asashiro-Nishi, Kumatori-cho, Sennan-gun, Osaka 590-0494, Japan
E-mail: kato.shinya.7w@kyoto-u.ac.jp

Key words: ferrous ion, oxidative membrane damage, fibroblasts, lipid peroxidation, reactive oxygen species

Introduction

Regulated cell death pathways play critical roles in maintaining physiological homeostasis and contributing to disease progression. Among these pathways, ferroptosis has attracted considerable attention due to its distinctive mechanisms and pathological relevance. In addition to canonical ferroptotic cell death, iron-dependent lipid peroxidation can also cause sublethal oxidative membrane injury that affects cellular function without necessarily inducing ferroptosis. First identified by Dixon *et al* (1) in 2012, ferroptosis is a form of regulated cell death characterized by iron-dependent lipid peroxidation, primarily driven by reactive oxygen species via the Fenton reaction. This process is initiated by ferrous ions (Fe^{2+}), a key factor in ferroptosis. Ferroptosis is a promising strategy for cancer therapy, and efforts have been made to explore mechanisms that activate key regulatory pathways to induce ferroptosis. Elastin, an elastic protein in the dermis, has been shown to induce ferroptosis by inhibiting cystine transporters, reducing glutathione (GSH) synthesis, and promoting the generation of reactive oxygen species (2). As previously demonstrated., under X-ray irradiation, the administration of elastin decreases GSH levels and glutathione peroxidase 4 (GPX4) expression, thereby enhancing cell death in HeLa and adenocarcinoma cell lines and a tumor xenograft model (3). Previous studies have indicated that oxygen levels and iron modulation, including nanoform iron or iron chelators, influence ferroptosis in cancer cells under X-ray irradiation. Hyperbaric oxygen could sensitize radioresistant oral squamous cell carcinoma cells to X-rays by promoting ferroptosis and reducing tumor growth in xenograft mice (4). On the other hand, deferoxamine weakly binds free iron and inhibits ferroptosis in bone marrow nucleated cells of X-ray-irradiated mice, thereby facilitating hematopoiesis in bone marrow (5). A nanocarrier composed of a hyperbranched copolymer with $^1O_2$-sensitive linkers and a RAS-selective lethal agent triggers $^1O_2$-mediated GSH depletion and GPX4 inactivation, leading to ferroptotic cell death in breast cancer-bearing mice (6).

Fibroblasts are cells found in connective tissue and become activated by inflammatory cytokines when tissue damage occurs due to radiation (7). As fibroblasts play a central role

in radiation-induced fibrosis, wound healing and long-term normal tissue responses, understanding oxidative membrane injury in these cells is particularly relevant in radiobiology. Activated fibroblasts produce components such as collagen and fibronectin, which serve as scaffolds for cells in the damaged tissue, thereby promoting tissue regeneration (8). As previously demonstrated, when human fibroblasts were irradiated with 20 Gy X-rays, mitochondria-dependent energy metabolism increased, and the cells underwent cell-cycle arrest (9). Therapeutic levels of radiation have cytotoxic effects on most cancer cells, inhibiting proliferation and inducing apoptosis (10). Irradiation with X-rays causes DNA damage, triggers mitochondrial signaling and AMP-activated protein kinase activity, suppresses mitochondrial metabolism and increases reactive oxygen species production in lung fibroblasts cultured under 5 and 20% O_2 (11). Moreover, fibroblasts treated with a low dose of 550 μGy X-rays have been shown to exhibit increased cell proliferation and protein production (12).

Liposomes containing phosphatidylcholine hydroperoxide induce ferroptosis by targeting divalent metal transporter 1, which promotes lysosomal Fe^{2+} efflux in breast cancer cells and xenografts (13). Prussian blue (Fe^{3+}-CN^--Fe^{2+}) and hyaluronic acid-based nanoparticles have been shown to induce ferroptosis, enhancing therapeutic efficacy under 6 Gy X-rays in human lung carcinoma and melanoma cells (14). Liposomes have been used to induce ferroptosis under radiation exposure; however, their interactions with Fe^{2+} under X-rays remain poorly understood, and fundamental insights are lacking. In this context, simplified liposome systems provide a reductionist approach to isolate Fe^{2+}-driven lipid peroxidation at membrane surfaces, rather than to recapitulate full cellular ferroptosis pathways.

The author has recently investigated cell growth inhibition in glioblastoma and neuroblastoma cells using lithium carbonate or platinum nano colloids under X-rays (15-17). While X-rays generate free radicals from water radiolysis (18), the role of Fe^{2+} in promoting the oxidation of lipid membranes and ferroptosis-related oxidative membrane damage is yet to be clarified. Alternatively, liposomes serve as a lipid membrane model reflecting membrane lipid peroxidation in ferroptosis research. The present study employed liposomes composed of the unsaturated lipids, L-α-dioleoylphosphatidylcholine (DOPC) and L-α-dioleoylphosphatidylserine (DOPS), at an 8:2 molar ratio as a lipid membrane model, without cholesterol, proteins, or antioxidant enzymes. The present study focused on early oxidative membrane damage and lipid peroxidation as mechanistic events associated with ferroptosis, rather than on establishing definitive ferroptotic cell death. The present study investigated the impact of Fe^{2+} on cell membrane damage in human fibroblast OUMS-36T-1 cells treated with X-rays, complemented by model experiments on membrane lipid peroxidation and Fe^{2+} oxidation using DOPC/DOPS (8:2 mol/mol) liposomes.

Materials and methods

Cells and cell culture. The OUMS-36T-1 cell line, an *hTERT* gene-transfected normal human embryo fibroblast, was obtained from the JCRB cell bank (cat. no. JCRB1006.1). The OUMS-36T-1 cells were cultured in Dulbecco's modified Eagle's (DMEM) medium with L-glutamine (FUJIFILM Wako Pure Chemical Corp.) supplemented with 10% fetal bovine serum (S-FBS-NL-015; Serana Europe GmbH) and penicillin-streptomycin-amphotericin B suspension (FUJIFILM Wako Pure Chemical Corp.) at 37˚C with 5% CO_2.

Cell proliferation assay using WST-8. Cell proliferation was evaluated using the WST-8 assay, which utilises a water-soluble tetrazolium salt (19). The OUMS-36T-1 cells were seeded at 2,000 cells/well in a 96-well culture plate (Sumitomo Bakelite Co., Ltd.) with n=5 wells and incubated for 24 h at 37˚C with 5% CO_2. Ferrous chloride tetrahydrate (Fe^{2+}; FUJIFILM Wako Pure Chemical Corp.) or ferric chloride hexahydrate (Fe^{3+}; FUJIFILM Wako Pure Chemical Corp.) were administered at 0-40 μM. Fresh Fe^{2+} solutions were prepared immediately prior to each experiment to minimize spontaneous oxidation to Fe^{3+} under culture conditions. The cells were exposed to 4 Gy X-rays (CAX-150-20; Chubu Medical Co., Ltd.; 150 kV-20 mA, 1 mm Al + 0.1 mm Cu filters, 0.60 Gy/min) and incubated for 3 days at 37˚C with 5% CO_2. A single dose of 4 Gy was selected as a representative moderate-to-high dose commonly used in *in vitro* radiobiological studies to reliably induce oxidative stress (15), while maintaining sufficient cell viability for early mechanistic analyses. The medium was replaced with 5% of 2-(2-methoxy-4-nitrophenyl)-3-(4-nitrophenyl)-5-(2,4-disulfophenyl)-2H-tetrazolium (WST-8; Dojindo Laboratories) diluted with DMEM medium and incubated for 1.5 h at 37˚C with 5% CO_2. The absorbance at 450 nm, corresponding to the formation of yellowish-orange formazan resulting from the reduction of WST-8 by intracellular mitochondrial dehydrogenase, was measured using a multi-spectrophotometer (Viento; Dainippon Sumitomo Pharma Co., Ltd.). The cells were then stained with Hoechst 33342 (Dojindo Laboratories) at room temperature for 15 min and observed using a fluorescence microscope (BZ-X710; KEYENCE Corporation) at x200 magnification with Ex/Em: 350/461 nm.

Analysis of intracellular reactive oxygen species using dichlorodihydrofluorescein diacetate (DCFH-DA). Ferrous ion (Fe^{2+}) concentrations (0-40 μM) were selected based on preliminary concentration-response experiments (data not shown) assessing cell proliferation and oxidative stress. A concentration of 40 μM was used as a threshold condition that induces intracellular oxidative stress and lipid peroxidation without causing overt membrane rupture in the absence of X-ray irradiation. Intracellular reactive oxygen species levels were evaluated using DCFH-DA (20). The OUMS-36T-1 cells were seeded at 3,500 cells/well in a 96-well culture plate with n=5 wells and incubated as described above. The DCFH-DA solution (ROS Assay Kit-Highly Sensitive DCFH-DA; Dojindo Laboratories) was added to each well and incubated for 30 min at 37˚C with 5% CO_2. After aspirating the medium, Fe^{2+} was administered at 40 μM, either alone or combined with trisodium citrate dihydrate (FUJIFILM Wako Pure Chemical Corp.) or reduced glutathione (GSH; FUJIFILM Wako Pure Chemical Corp.) at 40-120 μM. Following incubation for 0.2 h at 37˚C with 5% CO_2, the cells were exposed to 4 Gy X-rays. The early time point (0.2 h) was selected to capture

immediate oxidative responses at the membrane level, prior to the onset of secondary transcriptional or cell-death-related processes. To prevent light-induced auto-oxidation of the probe, all experiments using DCFH-DA were performed on black plates with room lights turned off and under dark conditions. The fluorescence intensity was measured at 0.2 h following X-ray irradiation using a multimode microplate reader (TriStar LB941; Berthold Technologies GmbH & Co. KG) at Ex/Em: 485/535 nm. Fluorescence intensity indicates intracellular reactive oxygen species levels, since DCFH-DA is enzymatically converted to DCFH, which is rapidly oxidized by reactive oxygen species into the fluorescent products.

Membrane lipid peroxidation detection and lactate dehydrogenase leakage. The disruption of the cell membrane was assessed by membrane lipid peroxidation and lactate dehydrogenase leakage. The OUMS-36T-1 cells were seeded at 3,500 cells/well and incubated as mentioned in 2.2. Fe^{2+} was administered at 40 μM, either alone or combined with trisodium citrate dihydrate or reduced glutathione at 40-120 μM. N-(4-Diphenylphosphinophenyl)-N'-(3,6,9,12-tetraoxatridecyl) perylene-3,4,9,10-tetracarboxydiimide (Liperfluo, Dojindo Laboratories) was added to each well at 7.5 μmol/l for the detection of lipid hydroperoxides (21). Following 0.2 h of incubation at 37˚C with 5% CO_2, the cells were exposed to 4 Gy of X-rays. After 0.2 h, fluorescence intensity, which is proportional to lipid peroxide in membrane lipids, was measured at Ex/Em=485/535 nm with the multimode microplate reader TriStar LB941. This early measurement was intended to assess primary membrane lipid peroxidation induced by Fe^{2+} and X-rays.

On the other hand, following irradiation with 4 Gy X-rays, the cells were incubated for 21 h at 37˚C with 5% CO_2. The cell culture medium was then replaced with DMEM containing the cytotoxicity LDH assay kit (Dojindo Laboratories), and the mixture was incubated for 0.5 h at room temperature in the dark. The absorbance at 490 nm, which is proportional to lactate dehydrogenase leakage (22), was measured with the multi-spectrophotometer Viento (Dainippon Sumitomo Pharma, Co. Ltd.).

Preparation of liposomes. Liposomes composed of DOPC and DOPS at an 8:2 molar ratio were prepared by mixing 1,2-dioleoyl-sn-glycero-3-phosphocholine (DOPC; NOF Corp.) and 1,2-dioleoyl-sn-glycero-3-phospho-L-serine (DOPS; NOF Corp.). A phospholipid thin film was formed by evaporating the chloroform solution of DOPC/DOPS (8:2) under reduced pressure using a custom apparatus developed by Dr Yoshimura [image of the device is shown in a previous study by the author (23)]. The resulting film was rehydrated in phosphate-buffered saline at pH 7.2 (PBS (-), FUJIFILM Wako Pure Chemical Corp.). The average particle diameter and zeta potential were 134 nm and -15.3 mV, respectively, as measured using a zeta potential and particle size analyzer (ELSZ-2; Otsuka Electronics Co. Ltd.).

Analysis of membrane lipid peroxidation using Liperfluo. The DOPC/DOPS (8:2) liposomes were added at 100 μM in a 96-well culture plate with n=5 wells. Fe^{2+} or Fe^{3+} was added at 0-50 μM, and Liperfluo was added to each well at 7.5 μmol/l. The plate was left to stand for 0.5 h, and then exposed to 4 Gy of X-rays. After 0.2 h, the fluorescence intensity was measured as described above.

Oxidation of ferrous ion using the Nitroso-PSAP method. The DOPC/DOPS (8:2) liposomes were added at 100 μM in a 1/2 area 96-well plate (UV-STAR; Greiner Bio-One International GmbH) with n=5 wells. Assays were performed under conditions containing or lacking the DOPC/DOPS (8:2) liposomes. Fe^{2+} or Fe^{3+} was added at 50 μM, and nitroso-N, N-dimethyl-p-phenylenediamine (Nitroso-PSAP; Dojindo Laboratories) was added to each well at 0.004 w/v% for the detection of ferrous ions (Fe^{2+}) (24). The plate was left to stand for 0.2 h, and then exposed to 4 Gy X-rays. After 0.2 h, the absorbance at 750 nm, corresponding to the residual ferrous ions (Fe^{2+}), was measured using the multi-spectrophotometer Viento (Dainippon Sumitomo Pharma, Co. Ltd.).

Statistical analysis. Data are presented as the mean ± standard deviation (SD), n=5 wells. Statistical analyses were performed using one-way analysis of variance (ANOVA) followed by Tukey's honestly significant difference (HSD) test for comparisons with the corresponding control group. For two-group comparisons, the Student's t-test was used. A value of $P<0.05$ was considered to indicate a statistically significant difference.

Results

The present study investigated the effects of X-rays on iron-dependent oxidative membrane damage relevant to ferroptosis by assessing intracellular levels of reactive oxygen species, membrane lipid peroxidation and lactate dehydrogenase leakage from human fibroblasts treated with ferrous ion (Fe^{2+}) and X-rays.

Effects of Fe^{2+} and Fe^{3+} on cell proliferation. Cell proliferation increased to 145.8% as the concentration of Fe^{2+} rose from 0 to 10 μM (Fig. 1), but decreased at higher concentrations, reaching 90.9% at 40 μM. Exposure to 4 Gy X-rays alone reduced cell proliferation to 85.6%. Combined treatment with Fe^{2+} and X-rays resulted in a concentration-dependent decline in cell proliferation, reaching a minimum of 26.5% at 40 μM. These trends were confirmed through fluorescence microscopy (Fig. 1). By contrast, ferric ion (Fe^{3+}) had a minimal effect on cell viability. Cell proliferation remained at 107.5% at 40 μM Fe^{3+} and decreased to 65.6% following X-ray irradiation, which was comparable to the untreated control (Fig. 1). This indicates that Fe^{3+} alone did not impair cell proliferation.

Effects of Fe^{2+} on the generation of intracellular reactive oxygen species, membrane lipid peroxidation and lactate dehydrogenase leakage. The present study then examined the effects of 40 μM Fe^{2+} on the generation of intracellular reactive oxygen species, membrane lipid peroxidation and lactate dehydrogenase leakage. Fe^{2+} was added extracellularly; however, based on the observed increases in intracellular reactive oxygen species and lipid peroxidation, it was hypothesized that Fe^{2+} may have contributed, directly or indirectly, to intracellular oxidative processes.

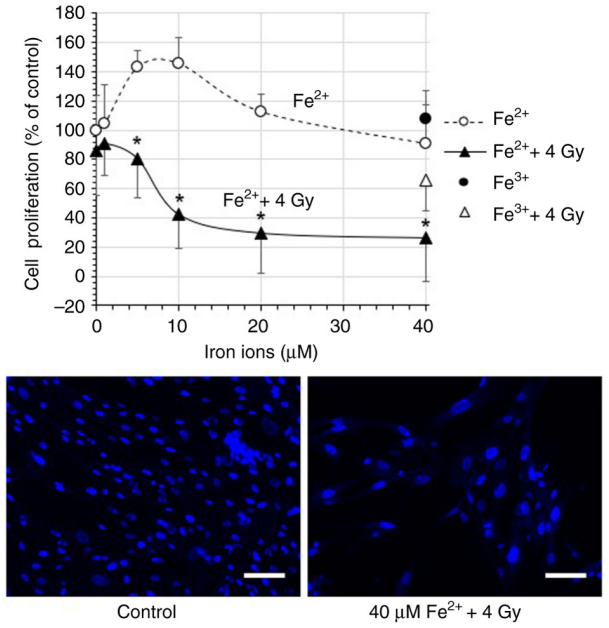

Figure 1. Proliferation of OUMS-36T-1 human fibroblasts. OUMS-36T-1 cells were treated with ferrous (Fe^{2+}) or ferric (Fe^{3+}) ions, followed by exposure to 4 Gy X-rays. After 3 days of incubation, cell proliferation was measured by mitochondrial dehydrogenase-reduced formazan-based WST-8 assay. Data are presented as the mean ± SD, n=5. *P<0.05 (vs. the corresponding non-irradiated control). Cell morphology was observed under a fluorescence microscope with Hoechst 33342 staining (Ex/Em: 350/461 nm) at x200 magnification. Scale bars, 100 μm. Fe^{2+}, ferrous ions; Fe^{3+}, ferric chloride hexahydrate.

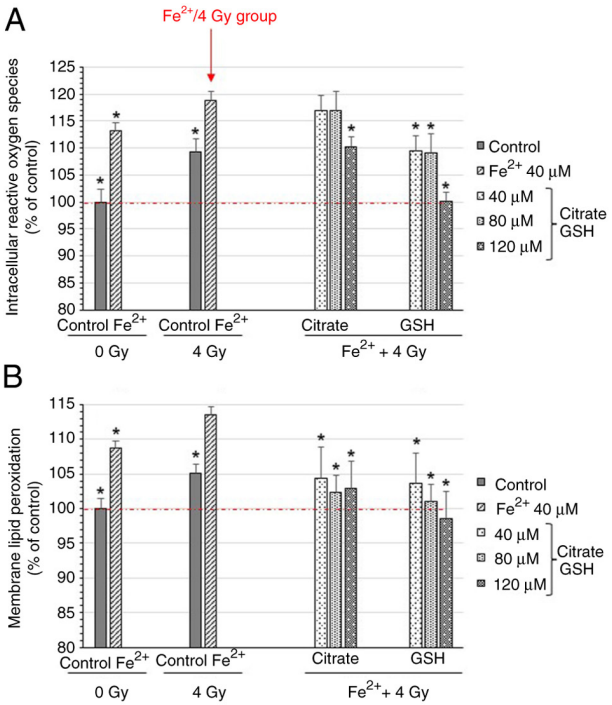

Figure 2. (A) Intracellular reactive oxygen species and (B) membrane lipid peroxidation in OUMS-36T-1 human fibroblasts. The OUMS-36T-1 cells were treated with ferrous (Fe^{2+}) ions at 40 μM, either alone or combined with trisodium citrate or reduced glutathione (GSH) at 40-120 μM, followed by exposure to 4 Gy X-rays. After 0.2 h, intracellular reactive oxygen species were assessed using DCFH-DA assay. Subsequently, in a separate experiment, following 0.2 h of incubation, hydroperoxide in the cell membrane was evaluated by measuring fluorescence intensity with the Liperfluo probe. Data are presented as the mean ± SD, n=5. Comparisons were made between the Fe^{2+} + 4 Gy group and all other experimental groups (*P<0.05). Fe^{2+}, ferrous ions.

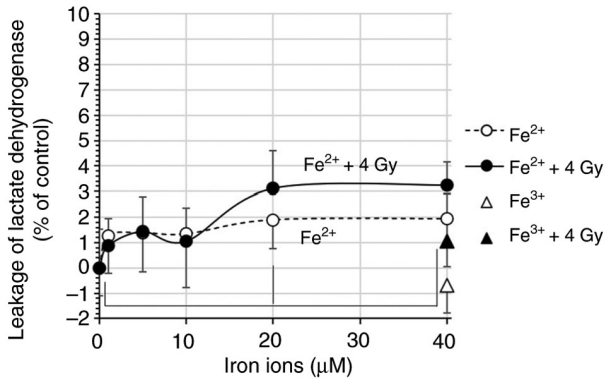

Figure 3. Cell membrane disruption in OUMS-36T-1 human fibroblasts. The OUMS-36T-1 cells were treated with ferrous (Fe^{2+}) or ferric (Fe^{3+}) ions, followed by exposure to 4 Gy X-rays. Following 21 h of incubation, cell membrane integrity was assessed using a lactate dehydrogenase leakage assay. Data are presented as the mean ± SD, n=5. Comparisons were made with the Fe^{2+} + 4 Gy group. Fe^{2+}, ferrous ions; Fe^{3+}, ferric chloride hexahydrate.

The levels of intracellular reactive oxygen species increased to 113.1% with Fe^{2+} alone and to 109.0% following X-ray irradiation (Fig. 2). The combination of Fe^{2+} and X-rays further elevated reactive oxygen species to 118.9%, suggesting a synergistic effect (Fig. 2). When trisodium citrate, a chelator of Fe^{2+}, was added at molar ratios of 1:1 to 1:3 (Fe^{2+}: citrate), intracellular reactive oxygen species decreased from 116.9 to 110.3%. Similarly, treatment with reduced GSH lowered intracellular reactive oxygen species from 109.4% to near baseline (Fig. 2).

A similar trend was observed in membrane lipid peroxidation. Treatment with 40 μM Fe^{2+} increased lipid peroxidation to 108.7%, and X-ray irradiation alone elevated it to 105.1% (Fig. 2). Combined treatment further increased it to 113.5%. Trisodium citrate and reduced GSH were more effective in suppressing lipid peroxidation than intracellular reactive oxygen species, reducing membrane lipid peroxidation to 102.9 and 98.5%, respectively (Fig. 2). These results indicate that Fe^{2+}-induced oxidative stress is especially significant near membrane surfaces or within lipid-rich microenvironments.

The leakage of lactate dehydrogenase, a marker for loss of membrane integrity, increased with rising concentrations of Fe^{2+}, reaching 1.9-fold at 40 μM (Fig. 3). When combined with X-rays, the lactate dehydrogenase leakage increased to 3.2-fold compared to the control, indicating exacerbated membrane disruption. Fe^{3+} at the same concentration did not increase lactate dehydrogenase leakage, further highlighting the distinct effects of Fe^{2+} (Fig. 3).

DOPC and DOPS model membranes. Subsequently, model membranes composed of DOPC and DOPS in an 8:2 molar ratio were prepared to investigate membrane-specific oxidative stress further. The resulting liposomes had an average diameter of 134 nm and a zeta potential of -15.3 mV (Fig. 4). The presence of anionic lipids such as DOPS likely facilitates electrostatic interactions with Fe^{2+}, while the unsaturated acyl chains of DOPC contribute to high membrane fluidity,

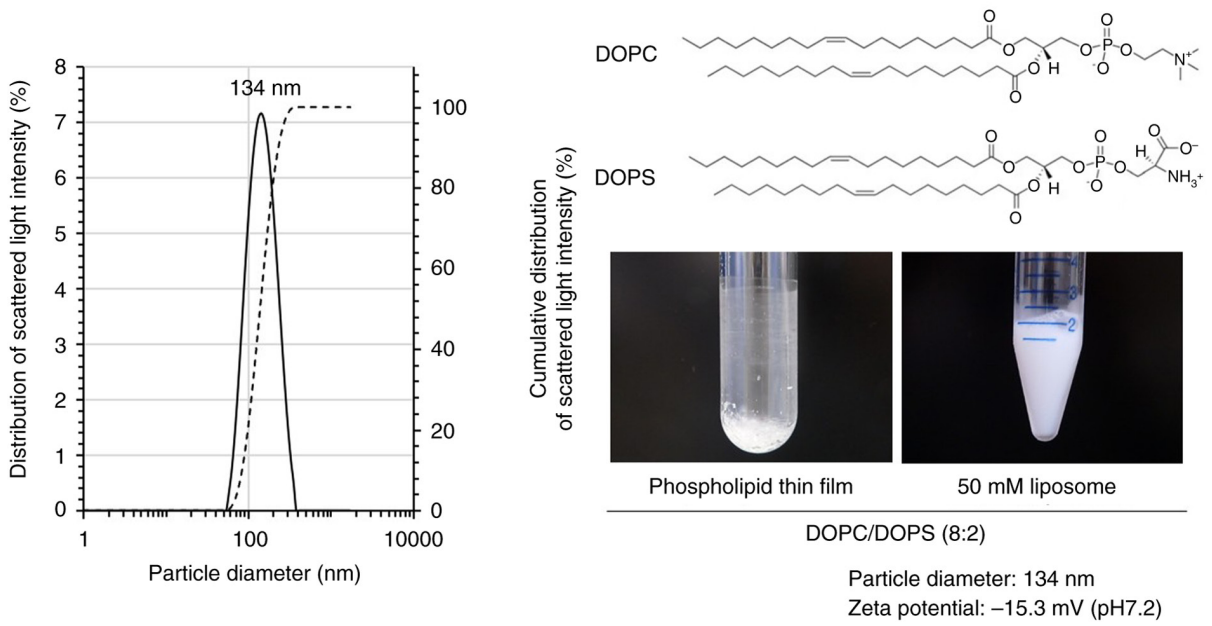

Figure 4. Preparation and characterization of DOPC/DOPS (8:2) liposomes. The DOPC/DOPS (8:2) liposomes were prepared by mixing DOPC and DOPS at a 8:2 molar ratio. A phospholipid thin film was formed by evaporating chloroform under reduced pressure, followed by redispersion in PBS (-) at pH 7.2. The mean particle diameter was 134 nm, and the zeta potential was -15.3 mV. DOPC, 1,2-dioleoyl-sn-glycero-3-phosphocholine; DOPS, 1,2-dioleoyl-sn-glycero-3-phospho-L-serine.

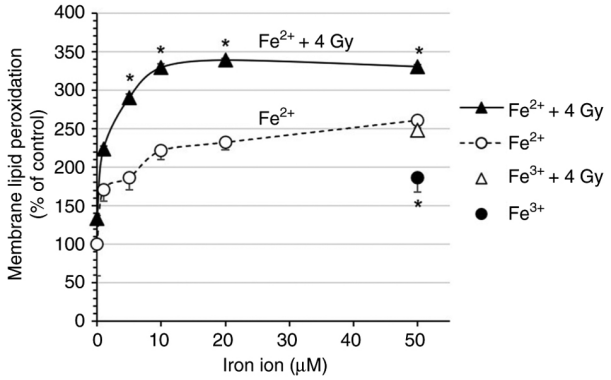

Figure 5. Lipid peroxidation in DOPC/DOPS (8:2) liposomes induced by Fe^{2+} and X-rays. The DOPC/DOPS (8:2) liposomes were treated with ferrous (Fe^{2+}) or ferric (Fe^{3+}) ions, followed by exposure to 4 Gy of X-rays. After 0.2 h, membrane lipid peroxidation was assessed by measuring fluorescence intensity with the Liperfluo probe. Data are presented as the mean ± SD, n=5. Statistical comparisons were made only between X-irradiated and non-irradiated groups at the same iron valence state (Fe^{2+} or Fe^{3+}) and at the same concentration (*P<0.05). Fe^{2+}, ferrous ions; Fe^{3+}, ferric chloride hexahydrate.

rendering the system more susceptible to lipid peroxidation. While lipid droplets have been proposed to buffer ferroptotic stress by sequestering iron or storing lipophilic antioxidants, our study focused on phospholipid bilayer liposomes as a model of membrane lipids. Thus, the observed effects mainly reflect direct Fe^{2+}/X-ray interactions with phospholipid membranes rather than lipid droplet-mediated mechanisms.

Effects of Fe^{2+} on lipid peroxidation. Lipid peroxidation in 100 μM liposomes, measured using Liperfluo, increased with Fe^{2+} treatment, reaching 261.1% at a concentration of 50 μM (Fig. 5). X-ray exposure alone increased peroxidation to 133.6%, and the combination of Fe^{2+} and X-rays further elevated it to 330.4%. Fe^{2+} induced a more modest increase and exhibited less synergy with X-rays, indicating that Fe^{2+} has greater redox activity under X-ray exposure.

To investigate the oxidation of Fe^{2+}, its residual concentration was measured using the Nitroso-PSAP method. A calibration curve was confirmed to be linear in the range of 0-80 μM we measured Fe^{2+} before measurements (Fig. 5). Upon adding 100 μM liposomes to 50 μM Fe^{2+}, the detectable amount of Fe^{2+} was 3.65 μM. X-ray exposure alone reduced Fe^{2+} to 2.95 μM, and the combination of liposomes and X-rays further reduced it to 1.80 μM (Fig. 6). Scatter plot data were fitted with linear trendlines, and the calibration curve shown in Fig. 6 was obtained using the linear regression (least-squares) function in Microsoft Excel.

Discussion

The results of the present study demonstrated that Fe^{2+} at low concentrations promoted fibroblast proliferation; however, at higher concentrations, it induced oxidative stress and membrane damage, with X-ray exposure amplifying these effects. By contrast, Fe^{3+} had a minimal effect, underscoring the distinct redox activity of Fe^{2+}. While the present study did not directly assess canonical ferroptosis markers, such as GPX4 or acyl-CoA synthetase long-chain family member 4 (ACSL4), the observed iron-dependent lipid peroxidation and membrane damage are consistent with early ferroptosis-related oxidative processes.

It is known that Fe^{2+} rapidly binds to intracellular proteins, such as ferritin and transferrin, thereby modulating its redox activity (25). These mechanisms may help explain the oxidative stress observed herein, although further experiments are required for direct validation. In addition, lysosomal iron release under oxidative stress has been reported as a potential

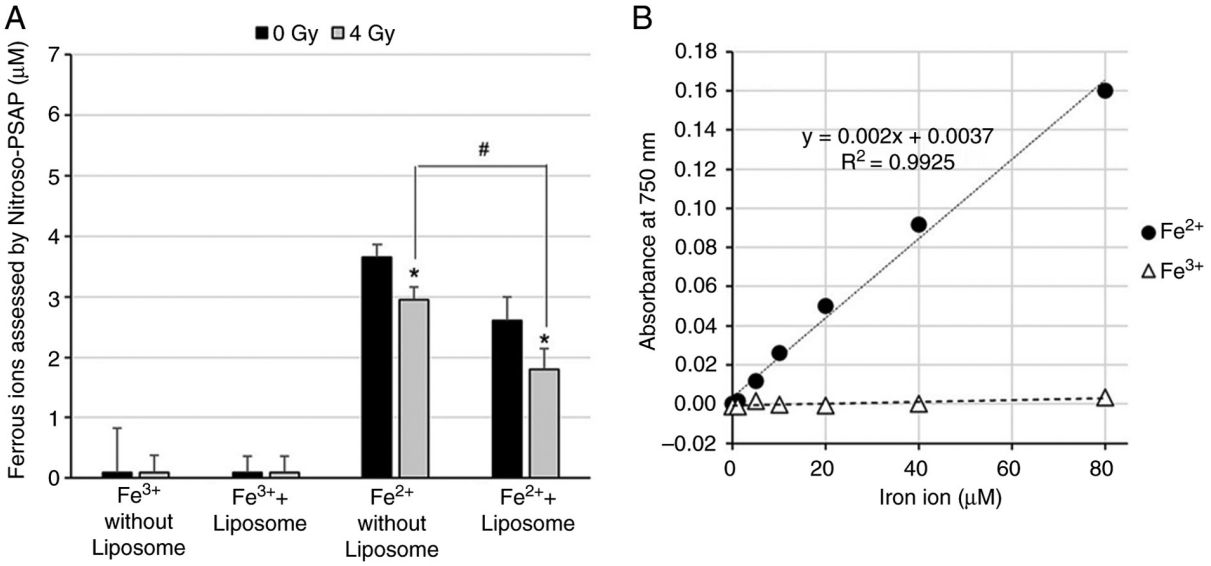

Figure 6. Oxidation of (Fe^{2+} in the presence of the DOPC/DOPS (8:2) Liposomes and Exposure to X-rays. The DOPC/DOPS (8:2) liposomes were treated with ferrous (Fe^{2+}) or ferric (Fe^{3+}) ions, followed by exposure to 4 Gy of X-rays. After 0.2 h, ferrous ion (Fe^{2+}) concentrations were quantified using the (A) Nitroso-PSAP method, and (B) with a calibration curve. Data are presented as the mean ± SD, n=5. $^{*}P<0.05$ (vs. non-irradiated samples) and $^{\#}P<0.05$ (Fe^{2+} vs. Fe^{2+}+ liposome). Fe^{2+}, ferrous ions; Fe^{3+}, ferric chloride hexahydrate.

contributor to cytosolic Fe^{2+} accumulation and lipid peroxidation (26,27). The results of the present study suggest that Fe^{2+} plays a central role in oxidative stress generation, likely via Fenton-type reactions (1,28). Although the present study did not verify lysosomal escape, future studies using lysosomal markers or inhibitors may clarify this mechanism.

Previous studies have reported that lipophilic antioxidants, such as ferrostatin-1 and liproxstatin-1 inhibit the Fe^{2+}-driven peroxidation of polyunsaturated phospholipids during ferroptosis (29). Although reduced GSH is a hydrophilic and non-lipid-permeable antioxidant, it significantly suppressed lipid peroxidation in the present study. It was noted that physiological intracellular reduced GSH concentrations are generally in the millimolar range (30), whereas the supplementation in the present study was at the micromolar level. The observed protective effect may therefore reflect localized antioxidant enhancement or the stabilization of extracellular Fe^{2+}, rather than a direct mimic of intracellular reduced GSH levels. This effect is likely attributable to the antioxidant properties of extracellular reduced GSH, which may scavenge reactive oxygen species generated under X-ray irradiation and Fe^{2+} exposure, thereby suppressing lipid peroxidation at the plasma membrane. Therefore, the GSH effects observed herein should be interpreted within the context of an *in vitro* model, rather than as a direct representation of intracellular antioxidant regulation.

Cell membranes, rich in polyunsaturated fatty acids, are highly susceptible to lipid peroxidation, a key trigger of ferroptosis following irradiation (31). It has been shown that 8 Gy X-rays induce significant membrane lipid peroxidation in human skin fibroblasts, as evidenced by the accumulation of malondialdehyde (32). Furthermore, X-ray exposure affects the utilization of reduced GSH and increases mitochondrial reactive oxygen species, ultimately disrupting cellular redox balance (33). Previous research using ultraviolet A has also demonstrated close associations among reactive oxygen species production, lipid peroxidation and lactate dehydrogenase leakage in fibroblasts (34). The findings of the present study are consistent with these reports, confirming that oxidative stress plays a central role in radiation-induced membrane damage. Notably, while Fe^{2+} alone induced oxidative stress and inhibited cell proliferation, significant membrane lipid peroxidation was only observed when Fe^{2+} was combined with X-ray irradiation, suggesting a synergistic cytotoxic effect.

The present study used DOPC/DOPS (8:2) liposomes as a model system to evaluate membrane-specific oxidative stress. These anionic, highly fluid membranes are expected to interact electrostatically with Fe^{2+}. They are prone to lipid peroxidation (23), allowing the focus on direct Fe^{2+}/X-ray effects on phospholipid bilayers, rather than lipid droplet-mediated mechanisms.

Consistent with this expectation, both Fe^{2+} and X-ray exposure enhanced lipid peroxidation, and their combination had a synergistic effect, whereas Fe^{3+} induced only modest changes. This indicates that Fe^{2+} possesses higher redox activity under X-rays and is a more potent driver of membrane damage. Notably, Fe^{2+} concentration measurements revealed accelerated oxidation to Fe^{3+} in the presence of membranes and X-rays, supporting the notion that phospholipid bilayers facilitate iron redox cycling. This behavior qualitatively resembles the mechanism of the Fricke dosimeter, in which irradiation drives the $Fe^{2+} \rightarrow Fe^{3+}$ conversion. These findings highlight that membrane environments are not passive targets, but active modulators of iron redox chemistry. Notably, previous research has shown that the Fenton reaction at air-water interfaces proceeds over 1,000 times faster than in bulk solution, producing high-valent iron-oxo species (Fe(IV)=O) without generating hydroxyl radicals (35). This is likely due to partial solvation and to increased accessibility of oxidants, such as hydrogen peroxide, to the iron center at the interface. In a related study, lactoferrin enhanced the Fenton reaction and increased hydroxyl

radical production under X-ray exposure (15), suggesting that iron-binding proteins may influence oxidative reactions in biological systems. In the present study, it was observed that X-ray exposure promoted Fe^{2+} oxidation in the presence of DOPC/DOPS (8:2) liposomes, supporting the hypothesis that cellular or membrane-like environments modulate redox reactions involving Fe^{2+}.

In cancer settings, such as clear cell renal cell carcinoma (ccRCC), the composition of lipid droplets (e.g., the enrichment of polyunsaturated fatty acids vs. monounsaturated fatty acids) and the accumulation of droplets have been reported to influence ferroptosis sensitivity (36,37). While the fibroblast and liposome system used herein does not directly address this mechanism, these findings highlight how membrane lipid composition can broadly shape susceptibility to ferroptosis. Furthermore, long non-coding RNAs (lncRNAs), such as LINC00336 and MALAT1 have been shown to regulate ferroptosis by sponging miRNAs in cancer models (38). In ccRCC, ferroptosis-related genes, such as ACSL4 have been identified as potential regulatory targets (39). Key effectors of ferroptosis, including GPX4 and ACSL4, may be regulated by lncRNA-miRNA networks in specific cancer contexts. Although these regulatory pathways were not addressed in the present fibroblast-based model, they illustrate how membrane lipid oxidation may intersect with broader ferroptosis regulatory networks in cancer contexts.

In summary, in the present study, Fe^{2+} promoted cell proliferation at low concentrations, whereas it induced oxidative stress and membrane damage at higher concentrations, effects that were amplified by X-ray exposure. Antioxidants suppressed these effects, and a liposome model confirmed that the membrane is involved in Fe^{2+} oxidation. These findings provide insight into ferroptosis mechanisms and highlight the therapeutic potential and environmental risks associated with iron and ionizing radiation.

In conclusion, the present study reveals a synergistic effect of Fe^{2+} and X-rays in promoting oxidative membrane damage in a fibroblast complemented by a liposome model. Fe^{2+} induces lipid peroxidation through membrane interactions, impairing cell proliferation, while X-rays amplify this oxidative stress. Given the essential role of fibroblasts in tissue regeneration, these findings underscore the biological importance of Fe^{2+}-mediated damage exacerbated by radiation. This insight contributes to a more in-depth understanding of iron-dependent oxidative mechanisms relevant to ferroptosis and may inform future strategies exploring ferroptosis-targeted cancer therapies under radiation exposure. Further *in vivo* studies and antioxidant evaluations are required to advance therapeutic and environmental applications.

Acknowledgements

The author would like to express his sincere gratitude to Mie University (Tsu, Japan), particularly the Radioisotope Experimental Facility and its dedicated staff, for providing a supportive environment that enabled this research. The author is also grateful to the Kanagawa Institute of Industrial Science and Technology (KISTEC) for their invaluable assistance with the particle size and zeta potential measurements of liposomes, and to Emeritus Professor Tetsuro Yoshimura (Mie University) for developing the liposome production apparatus and for his kind guidance on the liposome preparation method.

Funding

No funding was received.

Availability of data and materials

The data generated in the present study may be requested from the corresponding author.

Author's contributions

SK was involved in the conceptualization of the study, as well as in the study methodology, and investigation, and in the writing of the manuscript. SK confirms the authenticity of all the raw data. The author has read and approved the final manuscript.

Ethics approval and consent to participate

Not applicable.

Patient consent for publication

Not applicable.

Competing interests

The author declares that he has no competing interests.

References

1. Dixon SJ, Lemberg KM, Lamprecht MR, Skouta R, Zaitsev EM, Gleason CE, Patel DN, Bauer AJ, Cantley AM, Yang WS, *et al*: Ferroptosis: an iron-dependent form of nonapoptotic cell death. Cell 149: 1060-1072, 2012.
2. Dixon SJ, Patel DN, Welsch M, Skouta R, Lee ED, Hayano M, Thomas AG, Gleason CE, Tatonetti NP, Slusher BS and Stockwell BR: Pharmacological inhibition of cystine-glutamate exchange induces endoplasmic reticulum stress and ferroptosis. Elife 3: e02523, 2014.
3. Shibata Y, Yasui H, Higashikawa K, Miyamoto N and Kuge Y: Erastin, a ferroptosis-inducing agent, sensitised cancer cells to X-ray irradiation via glutathione starvation in vitro and in vivo. PLoS One 14: e0225931, 2019.
4. Liu J, An W, Zhao Q, Liu Z, Jiang Y, Li H and Wang D: Hyperbaric oxygen enhances X-ray induced ferroptosis in oral squamous cell carcinoma cells. Oral Dis 30: 116-127, 2024.
5. Zhang X, Wu Z, Lan H, Chen S, Wu J, Zhu L and Xiao Y: Deferoxamine promotes recovery of bone marrow hematopoietic function in mice exposed to a sublethal dose of X-ray irradiation. Nan Fang Yi Ke Da Xue Xue Bao 43: 1577-1584, 2023 (In Chinese).
6. Zhang B, Liu H, Wang Y, Zhang Y and Cheng J: Application of singlet oxygen-activatable nanocarriers to boost X-ray-induced photodynamic therapy and cascaded ferroptosis for breast cancer treatment. J Mater Chem B 11: 9685-9696, 2023.
7. Citrin DE, Prasanna PGS, Walker AJ, Freeman ML, Eke I, Barcellos-Hoff MH, Arankalayil MJ, Cohen EP, Wilkins RC, Ahmed MM, *et al*: Radiation-induced fibrosis: mechanisms and opportunities to mitigate. report of an NCI workshop, September 19, 2016. Radiat Res 188: 1-20, 2017.
8. Müller K and Meineke V: Radiation-induced alterations in cytokine production by skin cells. Exp Hematol 35 (Suppl 1): S96-S104, 2007.

9. Hirose E, Noguchi M, Ihara T and Yokoya A: Mitochondrial metabolism in X-Irradiated cells undergoing irreversible cell-cycle arrest. Int J Mol Sci 24: 1833, 2023.
10. Busato F, Khouzai BE and Mognato M: Biological mechanisms to reduce radioresistance and increase the efficacy of radiotherapy: State of the art. Int J Mol Sci 23: 10211, 2022.
11. Shimura T, Totani R, Ogasawara H, Inomata K, Sasatani M, Kamiya K and Ushiyama A: Effects of oxygen on the response of mitochondria to X-irradiation and reactive oxygen species-mediated fibroblast activation. Int J Radiat Biol 99: 769-778, 2023.
12. Truong K, Bradley S, Baginski B, Wilson JR, Medlin D, Zheng L, Wilson RK, Rusin M, Takacs E and Dean D: The effect of well-characterized, very low-dose x-ray radiation on fibroblasts. PLoS One 13: e0190330, 2018.
13. Jiang J, Yang L, Xie Q, Liu X, Jiang J, Zhang J, Zhang S, Zheng H, Li W, Cai X, *et al*: Synthetic vectors for activating the driving axis of ferroptosis. Nat Commun 15: 7923, 2024.
14. Bae C, Hernández Millares R, Ryu S, Moon H, Kim D, Lee G, Jiang Z, Park MH, Kim KH, Koom WS, *et al*: Synergistic effect of ferroptosis-inducing nanoparticles and X-Ray irradiation combination therapy. Small 20: e2310873, 2024.
15. Kato S: Lactoferrin inhibits the proliferation of IMR-32 neuroblastoma cells even under X-rays. Med Int (Lond) 3: 33, 2023.
16. Kato S: Effects of platinum-coexisting dopamine with X-ray irradiation upon human glioblastoma cell proliferation. Hum Cell 34: 1653-1661, 2021.
17. Kato S: Under lithium carbonate administration, nicotine triggers cell dysfunction in human glioblastoma U-251MG cells, which is distinct from cotinine. Med Int (Lond) 2: 19, 2022.
18. Jay-Gerin JP: Fundamentals of Water Radiolysis. Encyclopedia 5: 38, 2025.
19. Ishiyama M, Tominaga H, Shiga M, Sasamoto K, Ohkura Y and Ueno K: A combined assay of cell viability and in vitro cytotoxicity with a highly water-soluble tetrazolium salt, neutral red and crystal violet. Biol Pharm Bull 19: 1518-1520, 1996.
20. Eruslanov E and Kusmartsev S: Identification of ROS using oxidized DCFDA and flow-cytometry. Methods Mol Biol 594: 57-72, 2010.
21. Soh N, Ariyoshi T, Fukaminato T, Nakajima H, Nakano K and Imato T: Swallow-tailed perylene derivative: A new tool for fluorescent imaging of lipid hydroperoxides. Org Biomol Chem 5: 3762-3768, 2007.
22. Kumar P, Nagarajan A and Uchil PD: Analysis of cell viability by the lactate dehydrogenase assay. Cold Spring Harb Protoc: Jun 1, 2018 (Epub ahead of print).
23. Kato S and Kuwata K: Pro-/anti-oxidative properties of dopamine on membrane lipid peroxidation upon X-ray irradiation. Radiat Phys Chem 185: 109518, 2021.
24. El Behery M, Fujimura M, Kimura T and Tsubaki M: Direct measurements of ferric reductase activity of human 101F6 and its enhancement upon reconstitution into phospholipid bilayer nanodisc. Biochem Biophys Rep 21: 100730, 2020.
25. Muckenthaler MU, Rivella S, Hentze MW and Galy B: A red carpet for iron metabolism. Cell 168: 344-361, 2017.
26. Cañeque T, Baron L, Müller S, Carmona A, Colombeau L, Versini A, Solier S, Gaillet C, Sindikubwabo F, Sampaio JL, *et al*: Activation of lysosomal iron triggers ferroptosis in cancer. Nature 642: 492-500, 2025.
27. Stockwell BR, Friedmann Angeli JP, Bayir H, Bush AI, Conrad M, Dixon SJ, Fulda S, Gascón S, Hatzios SK, Kagan VE, *et al:* Ferroptosis: A regulated cell death nexus linking metabolism, redox biology, and disease. Cell 171: 273-285, 2017.
28. Yang WS and Stockwell BR: Ferroptosis: Death by lipid peroxidation. Trends Cell Biol 26: 165-176, 2016.
29. Zilka O, Shah R, Li B, Friedmann Angeli JP, Griesser M, Conrad M and Pratt DA: On the mechanism of cytoprotection by ferrostatin-1 and Liproxstatin-1 and the role of lipid peroxidation in ferroptotic cell death. ACS Cent Sci 3: 232-243, 2017.
30. Montero, D, Tachibana C, Rahr Winther J and Appenzeller-Herzog C: Intracellular glutathione pools are heterogeneously concentrated. Redox Biol 1: 508-513, 2013.
31. Mao C, Lei G, Horbath A and Gan B: Assessment of lipid peroxidation in irradiated cells. Methods Cell Biol 172: 37-50, 2022.
32. Kim BC, Shon BS, Ryoo YW, Kim SP and Lee KS: Melatonin reduces X-ray irradiation-induced oxidative damages in cultured human skin fibroblasts. J Dermatol Sci 26: 194-200, 2001.
33. Shimura T, Nakashiro C, Fujiwara K, Shiga R, Sasatani M, Kamiya K and Ushiyama A: Radiation affects glutathione redox reaction by reduced glutathione peroxidase activity in human fibroblasts. J Radiat Res 63: 183-191, 2022.
34. Morlière P, Moysan A, Santus R, Hüppe G, Mazière JC and Dubertret L: UVA-induced lipid peroxidation in cultured human fibroblasts. Biochim Biophys Acta 1084: 261-268, 1991.
35. Enami S, Sakamoto Y and Colussi AJ: Fenton chemistry at aqueous interfaces. Proc Natl Acad Sci USA 111: 623-628, 2014.
36. Kim JW, Lee JY, Oh M and Lee EW: An integrated view of lipid metabolism in ferroptosis revisited via lipidomic analysis. Exp Mol Med 55: 1620-1631, 2023.
37. Klasson TD, LaGory EL, Zhao H, Huynh SK, Papandreou I, Moon EJ and Giaccia AJ: ACSL3 regulates lipid droplet biogenesis and ferroptosis sensitivity in clear cell renal cell carcinoma. Cancer Metab 10: 14, 2022.
38. Wang M, Mao C, Ouyang L, Liu Y, Lai W, Liu N, Shi Y, Chen L, Xiao D, Yu F, *et al*: Long noncoding RNA LINC00336 inhibits ferroptosis in lung cancer by functioning as a competing endogenous RNA. Cell Death Differ 26: 2329-2343, 2019.
39. Guo N: Identification of ACSL4 as a biomarker and contributor of ferroptosis in clear cell renal cell carcinoma. Transl Cancer Res 11: 2688-2699, 2022.